

Supporting Information

Role of Short-Range Chemical Ordering in (GaN)_{1-x}(ZnO)_x for Photo-driven Oxygen Evolution

Dennis P. Chen,[†] Joerg C. Neufeind,[‡] Kallum M. Koczkur,[†] David L. Bish,[§] and Sara E. Skrabalak^{†*}

[†]Department of Chemistry, Indiana University - Bloomington, 800 East Kirkwood Avenue, Bloomington, Indiana 47405, USA

[‡]Chemical and Engineering Materials Division, Oak Ridge National Laboratory, Oak Ridge, Tennessee 37831, USA

[§]Department of Geological Sciences, Indiana University, 1001 East 10th Street, Bloomington, Indiana 47405, USA

Table of Content

Content Description	Page
Table S1. Description of reaction conditions and energy-dispersive X-ray spectroscopy (EDS) analysis of GZNO samples	S3
Figure S1. Photograph of the crude mixture of a GZNO nitridation reaction and EDS analysis comparing the Zn content of GZNO-buff sampled from various locations in the reaction boat	S4
Figure S2. Powder X-ray diffraction (XRD) patterns of the as-nitridated mixture and acid-washed GZNO-buff	S5
Figure S3. Irradiance spectrum of the Xe arc lamp	S5
Figure S4. Scanning electron microscopy (SEM) micrographs of the GZNO reaction series	S6
Figure S5. Comparative X-ray photoelectron spectroscopy (XPS) analysis of GZNO synthesized with (GZNO-buff) and without (GZNO-nobuff) a ZnO buffer layer	S6
Figure S6. Rietveld refinements of neutron diffraction data for the GZNO temperature series	S7
Table S2. Crystallographic and atomic parameters from Rietveld refinements of neutron diffraction data for the GZNO temperature series	S8
Figure S7. Rietveld refinements of synchrotron diffraction data for the GZNO reaction series	S9

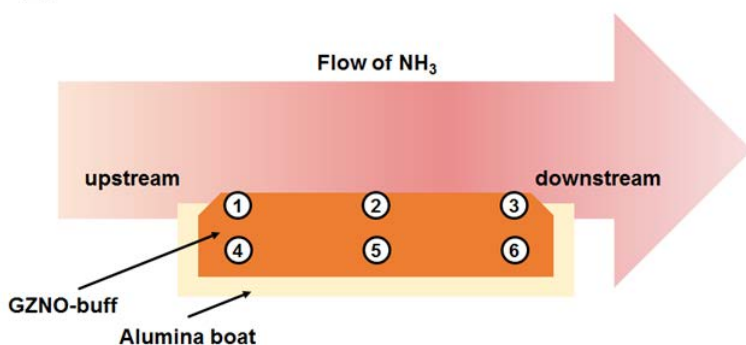
Figure S8. Normalized total-scattering patterns ($S(Q)-1$) of GZNO samples obtained from summed NOMAD data	S10
Figure S9. Comparison of atomic PDF refinements with various unit-cell models	S11
Figure S10. Reverse Monte-Carlo (RMC) refinements and partial-pair-distribution functions for the GZNO reaction series	S12
Table S3. RMC tabulated residuals for the GZNO reaction series	S13
Figure S11. RMC refinements for the GZNO temperature series	S13
Table S4. RMC tabulated residuals for the GZNO temperature series	S14
Figure S12. Representative selected-area electron-diffraction (SAED) patterns of GZNO-buff and corresponding simulated patterns	S15
Figure S13. GZNO unit-cell parameters	S16
Figure S14. Urbach fits of diffuse-reflectance (DR) spectra of GZNO samples and corresponding Tauc plots	S17
Figure S15. N_2 adsorption and desorption isotherms of GZNO samples tested for the O_2 -evolution half-reaction	S18
References	S18

Table S1. Description of reaction conditions and EDS analysis of GZNO samples. The Zn and Ga content of GZNO-buff and GZNO-nobuff were obtained using inductively coupled plasma optical emission (ICP-OES) spectrometry in which values of 0.64 ± 0.01 and 0.40 ± 0.01 for Zn/(Zn+Ga) were obtained, respectively. Considering the similarity between the Zn content obtained from EDS and ICP-OES analyses, EDS-derived values were used as a proxy for the nominal metal content in GZNO.

Sample	Sample Description	Zn / (Zn + Ga)
<u>Reaction Series</u>		
GZNO-SSR	Precursors: Ga ₂ O ₃ + ZnO Reaction: 15 h at 850 °C, under NH ₃ (300 sccm)	0.09
GZNO-nobuff	Precursors: ZnGa-LDH Reaction: 10 h at 800 °C, under O ₂ /NH ₃ (15/800 sccm)	0.41
GZNO-buff	Precursors: ZnGa-LDH + ZnO Reaction: 10 h at 800 °C, under O ₂ /NH ₃ (15/800 sccm)	0.66
<u>Temperature Series</u>		
GZNO-700	Precursors: ZnGa-LDH + ZnO Reaction: 20 h at 700 °C, under O ₂ /NH ₃ (15/800 sccm)	0.66
GZNO-750	Precursors: ZnGa-LDH + ZnO Reaction: 15 h at 750 °C, under O ₂ /NH ₃ (15/800 sccm)	0.65
GZNO-1000	Precursors: ZnGa-LDH + ZnO Reaction: 10 min at 1000 °C, O ₂ /NH ₃ (15/800 sccm)	0.55



B



C

Position	Zn / (Zn + Ga)
<u>Top Layer</u>	
1	0.65
2	0.66
3	0.66
<u>Bottom Layer</u>	
4	0.63
5	0.63
6	0.65

Figure S1. (A) Photograph of the crude product of a typical GZNO nitridation with the portion of the top ZnO:N layer peeled off. The orange and black microcrystals correspond to the desired GZNO phase and ZnO:N byproduct, respectively. (B) Positions in which GZNO-buff particles were sampled and characterized by EDS analysis; (C) Corresponding Zn fractions obtained from EDS analysis. The average Zn fraction obtained from EDS analysis of the unwashed crude obtained from position 1, 3, 4, and 6 was 0.70 ± 0.01 .

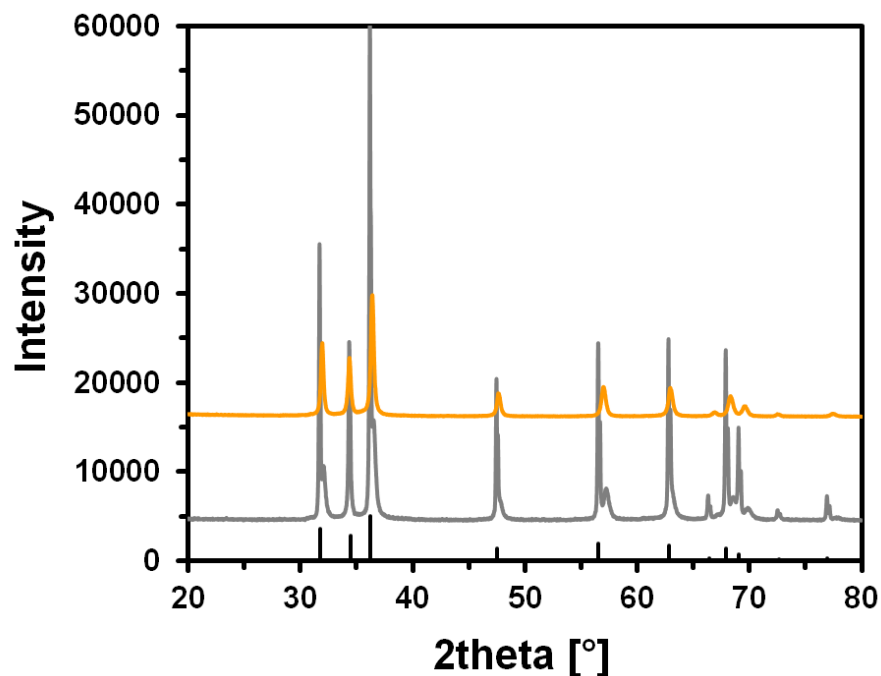


Figure S2. Laboratory powder XRD patterns of the as-nitridated mixture (gray) and acid-washed GZNO-buff (orange). Two distinct phases are observed in the gray pattern. A ZnO reference pattern (ICDD: 00-005-0664) is shown as a comparison. The sharper of the two sets of reflections correspond to the ZnO:N phase, which appear to have larger crystallites (Figure S1A) than GZNO-buff. This observation is consistent with the sharper peaks and the peak positions in the ZnO:N pattern being shifted towards lower 2θ relative to the GZNO-buff pattern. After washing with 4 M HNO_3 , the ZnO:N reflections were no longer observed.

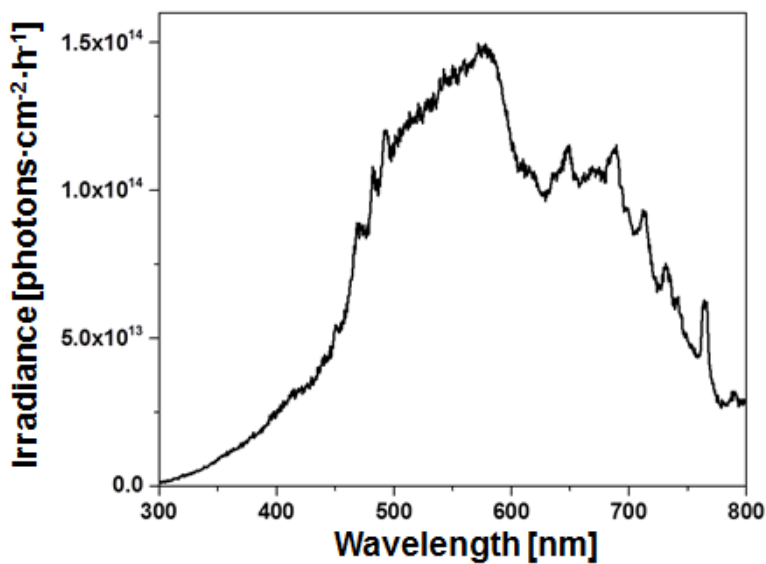


Figure S3. Irradiance spectrum of the Xe arc lamp (unfiltered) used for the photocatalysis measurements.

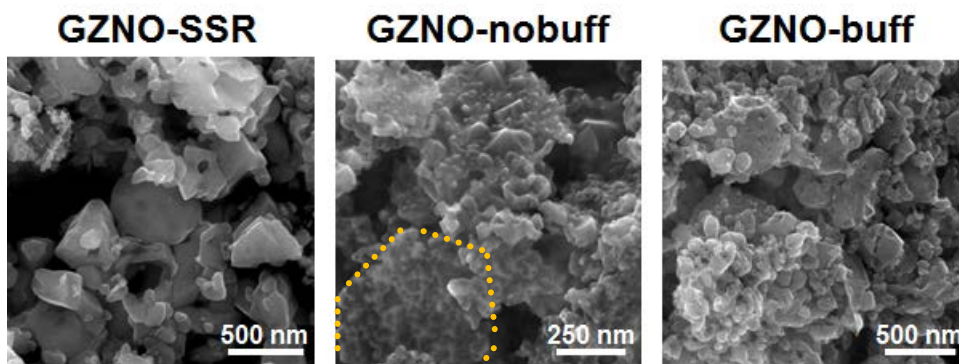


Figure S4. SEM micrographs of the GZNO reaction series.

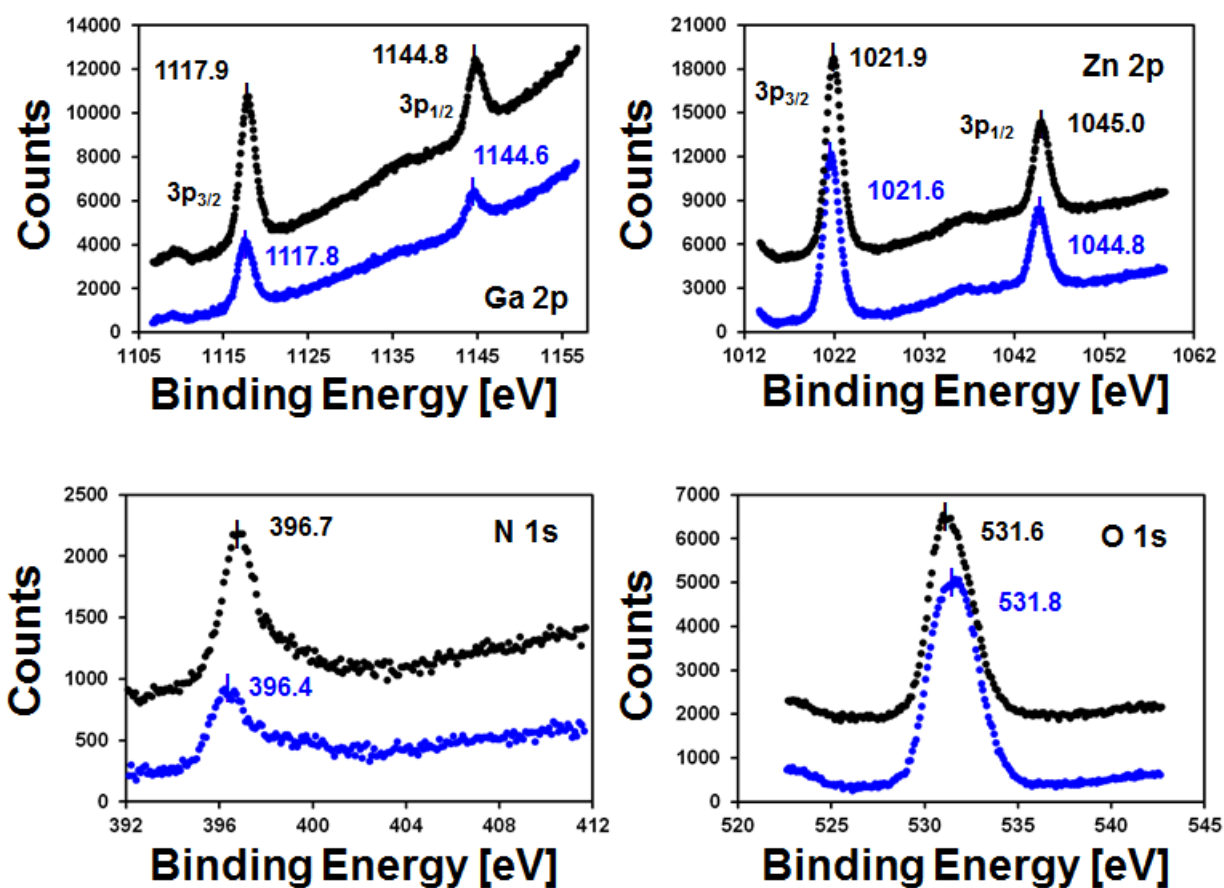


Figure S5. High-resolution XPS scans of the Ga 2p, Zn 2p, N 1s, and O 1s regions of GZNO-nobuff (black) and GZNO-buff (blue). Tick marks indicate the Gaussian-fitted peak-maximum.

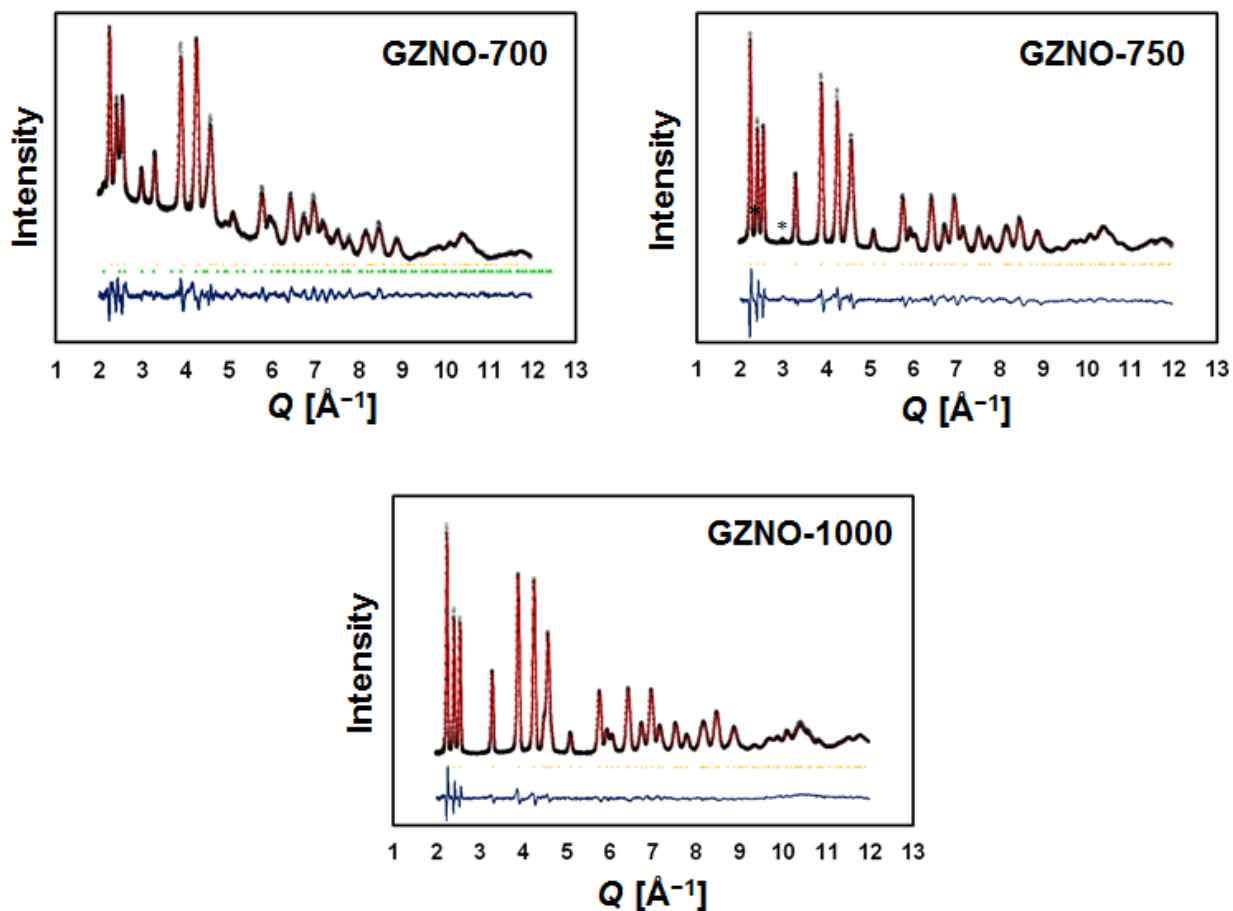


Figure S6. Structure models refined using NOMAD bank 3 ($2\theta = 65^\circ$, flight path = 20.64 m) data (normalized intensity) for the GZNO temperature series. Apart from the 700 °C dataset, only the wurtzite-structure type (space group $P6_3mc$) was used as the structure model for Rietveld refinement. To account for impurity peaks, the 700 °C powder pattern was fitted using a two-phase model using a Le Bail fit where the first and second phases were the wurtzite and spinel structure type, respectively. The observed intensity, calculated intensity, and difference plot are represented by the open markers, red line, and blue line, respectively. The tick marks below the Bragg pattern correspond to the hkl reflections from the wurtzite (yellow) and spinel (green) phases. The asterisk in the GZNO-750 pattern denotes a reflection originating from spinel-like impurities. Although an impurity phase is present in GZNO-750, its contribution to the local structure models appeared negligible and does not change the general conclusion of the discussions. Derived residual fits, unit-cell parameters, and atomic parameters are tabulated below (Table S2).

Table S2. Crystallographic and atomic parameters obtained from structure refinements for the GZNO temperature series. All refinements used normalized data obtained from NOMAD's bank number 3 ($2\theta = 65^\circ$, flight path = 20.64 m).

GZNO 700		$R_{wp} = 2.74$				
<i>P6₃mc</i> (186)						
a = 3.22718(22) c = 5.2240(5)						
Cell Vol. = 47.117(7)						
<i>Fd-3m:2</i> (227)						
a = 8.4044(28)						
Cell Vol. = 593.64(34)						
<hr/>						
GZNO-750		$R_{wp} = 6.33$				
<i>P6₃mc</i> (186)						
a = 3.23468(17) c = 5.2152(4)						
Cell Vol. = 47.257(5)						
Atom	X	y	z	U_{iso}	Occupancy	
Zn	1/3	2/3	0.3803(4)	0.0071(3)	0.65	
Ga	1/3	2/3	0.3803(4)	0.0071(3)	0.35	
O	1/3	2/3	0	0.00995(31)	0.65	
N	1/3	2/3	0	0.00995(31)	0.35	
<hr/>						
GZNO-1000		$R_{wp} = 8.97$				
<i>P6₃mc</i> (186)						
a = 3.22927(15) c = 5.2121(4)						
Cell Vol. = 47.071(4)						
Atom	x	y	z	U_{iso}	Occupancy	
Zn	1/3	2/3	0.3803(2)	0.0084(2)	0.55	
Ga	1/3	2/3	0.3803(2)	0.0084(2)	0.45	
O	1/3	2/3	0	0.0101(6)	0.55	
N	1/3	2/3	0	0.0101(6)	0.45	

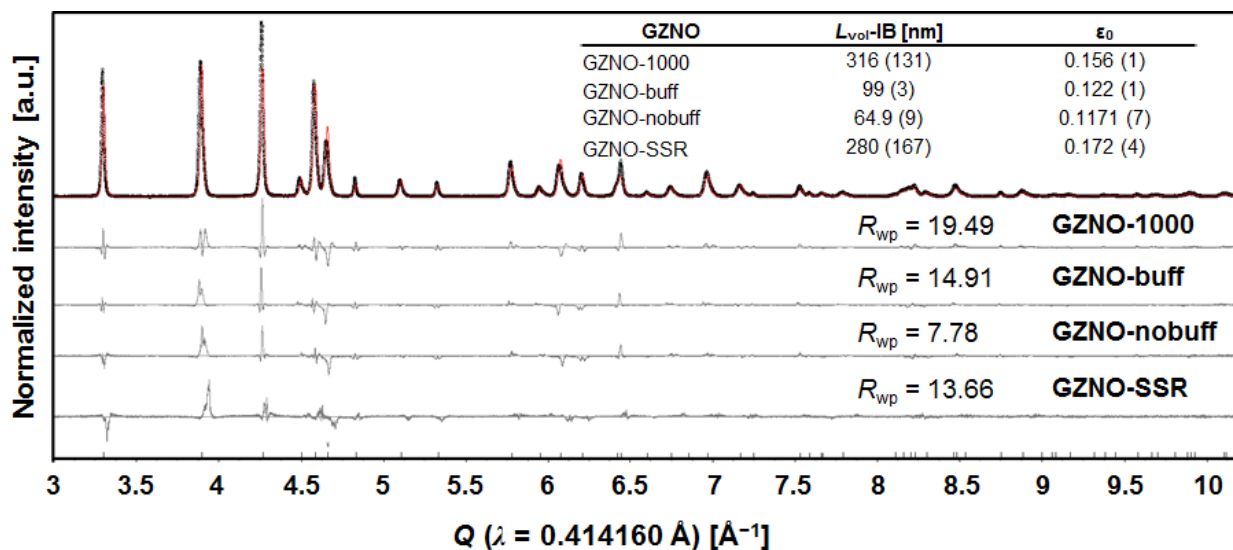


Figure S7. Results of Rietveld refinements using synchrotron diffraction data using a $P6_3mc$ structure model. Occupancies and atomic displacement parameters were fixed to values obtained from the neutron refinements. Microstructural parameters were obtained using the ‘Double-Voigt’ approach available in the GUI of *TOPAS v4.1*. The inset shows the volume weighted mean column height, $L_{\text{vol-IB}}$ and the upper limit to the apparent strain ϵ_0 .¹ The standard implementation of the Double-Voigt approach in *TOPAS v4.1* does not model anisotropic line-broadening, therefore the absolute values of the derived microstructure parameters should not be taken literally. Here the emphasis is placed on the relative difference between the samples.

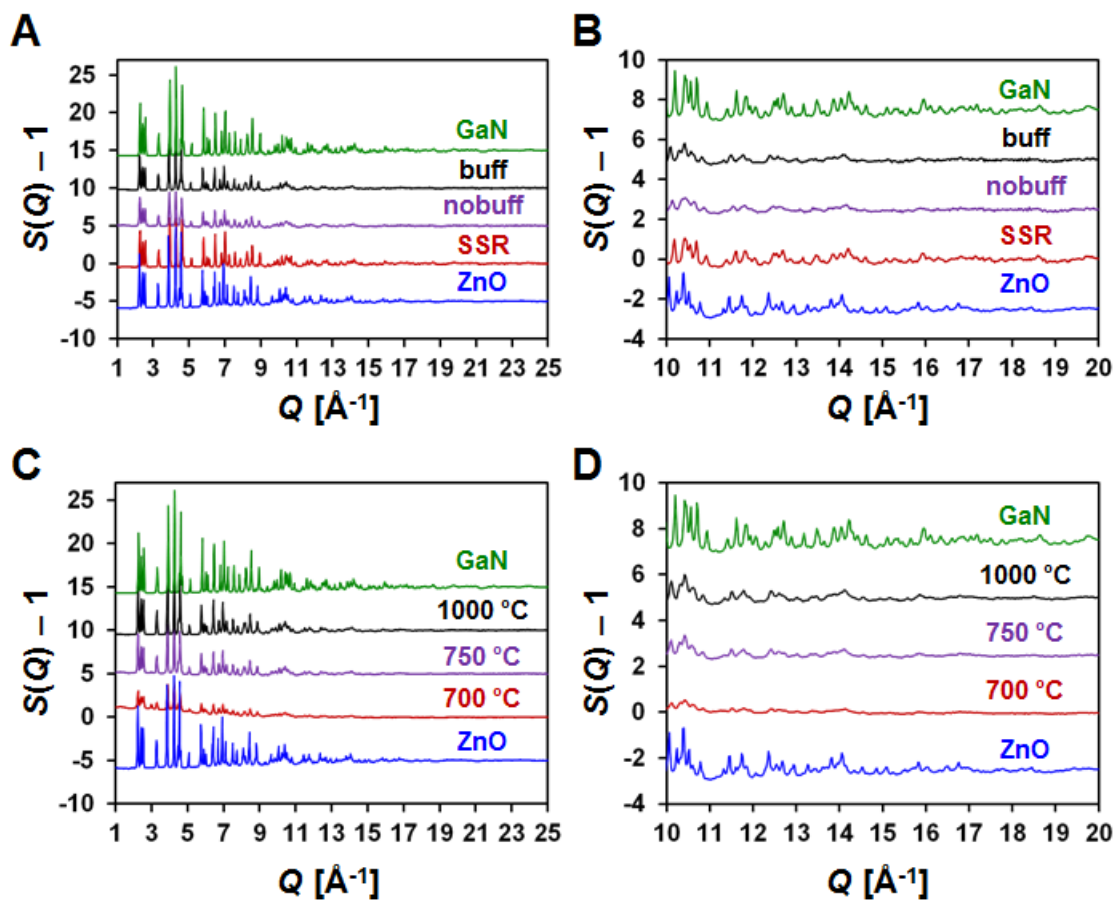


Figure S8. Normalized structure factor ($S(Q)-1$) of GZNO samples obtained from NOMAD. (A) and (C) display profiles for the GZNO reaction series and the GZNO temperature series, respectively. Panels (B) and (D) respectively correspond to an expanded plot of (A) and (C) for the Q -range 10–20 \AA^{-1} .

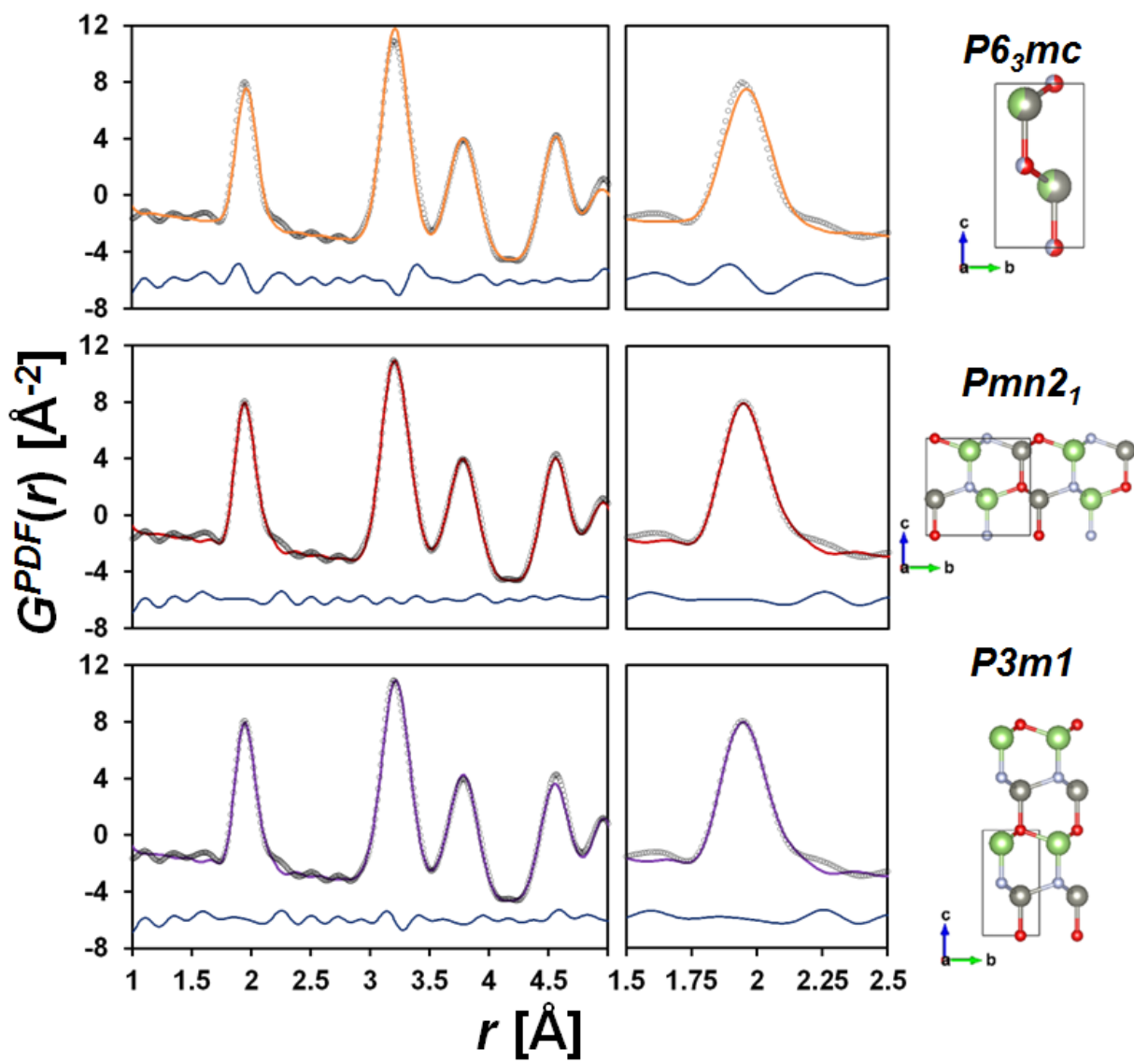


Figure S9. Fits to the neutron $G^{PDF}(r)$ for GZNO-buff against the high-symmetry wurtzite unit-cell ($P6_3mc$) and two lower symmetry hettotypes with spacegroups $Pmn2_1$ (orthorhombic, ordering along b -axis) and $P3m1$ (hexagonal, ordering along c -axis).

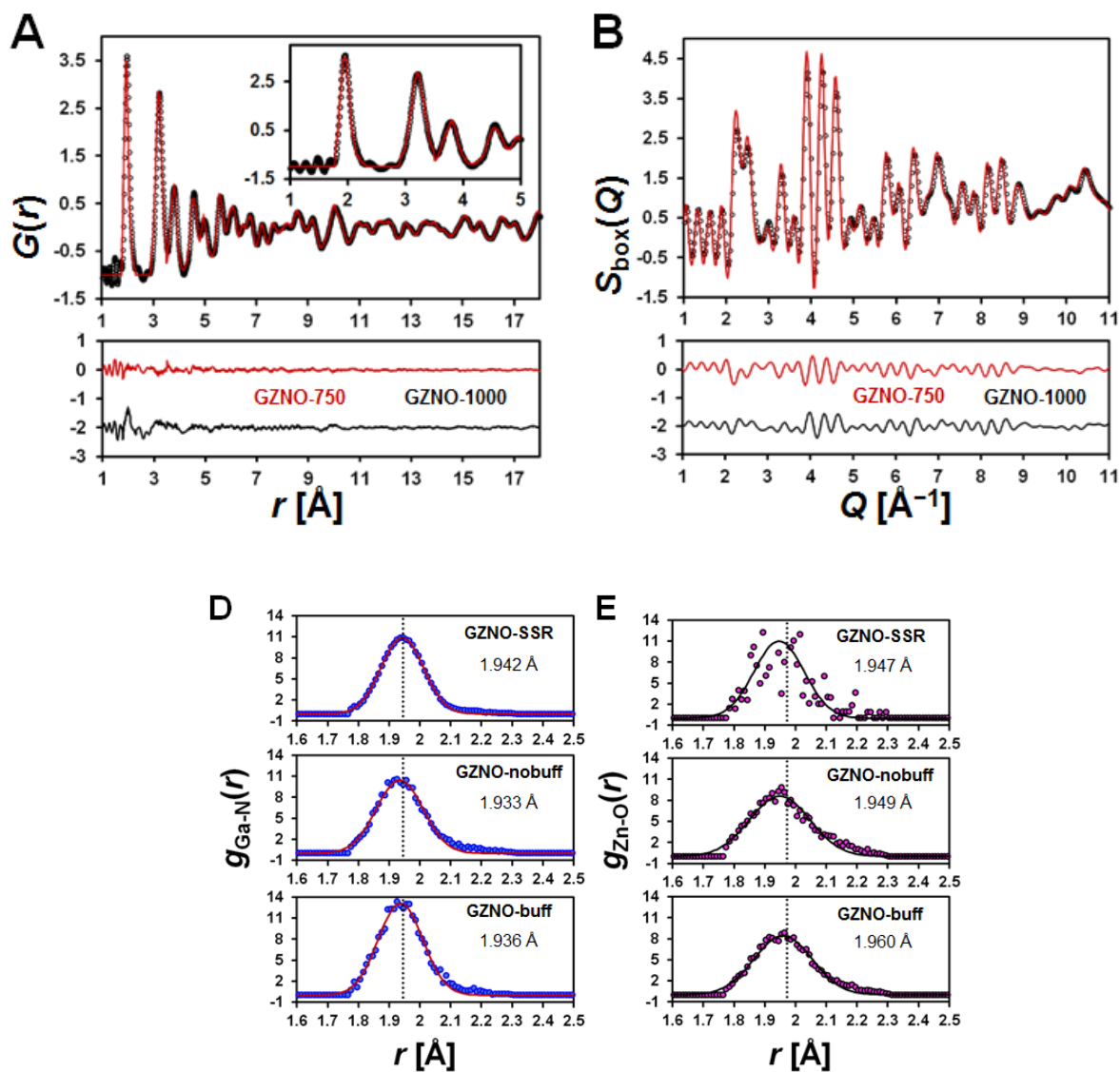


Figure S10. RMC refinement of the GZNO reaction series. (A) The experimental $G(r)$ of GZNO-buff (open circles) fitted to the calculated pattern derived from the RMC structure model (red trace). The difference plot between the experimental and calculated $G(r)$ for GZNO-buff, GZNO-nobuff, and GZNO-SSR is shown below the $G(r)$ plot. (B) The box-convolution of the experimental $S(Q)$ of GZNO-buff (open circles) fitted to the calculated pattern derived from the RMC structure model (red trace). The difference plot between the experimental and calculated $S(Q)$ for GZNO-buff, GZNO-nobuff, and GZNO-SSR is shown below the $S(Q)$ plot. (C) The nearest-neighbor pair-correlation functions, $g_{ij}(r)$ for the RMC structure model of GZNO-buff. (D) and (E) show the nearest-neighbor Ga–N and Zn–O $g_{ij}(r)$ for GZNO-buff.

Table S3. Residual values from the RMC refinement of the GZNO reaction series. Chi values from RMC refinements where the atom swapping was allowed were compared with refinements that had a random atomic arrangement and only allowed to translate.

Refinement	overall χ^2	Bragg χ^2	$G(r)$ χ^2	$S(Q)$ χ^2	BVS χ^2
GZNO-SSR	236.8	49.49	18.73	1674	0.0896
GZNO-SSR (random)	237.1	49.85	18.7	1676	0.0873
GZNO-nobuff	235.6	65.35	4.865	1660	0.15622
GZNO-nobuff (random)	237.5	67.48	4.897	1667	0.185
GZNO-buff	224.5	45.92	12.82	1626	0.15664
GZNO-buff (random)	225.4	46.83	12.83	1630	0.19272

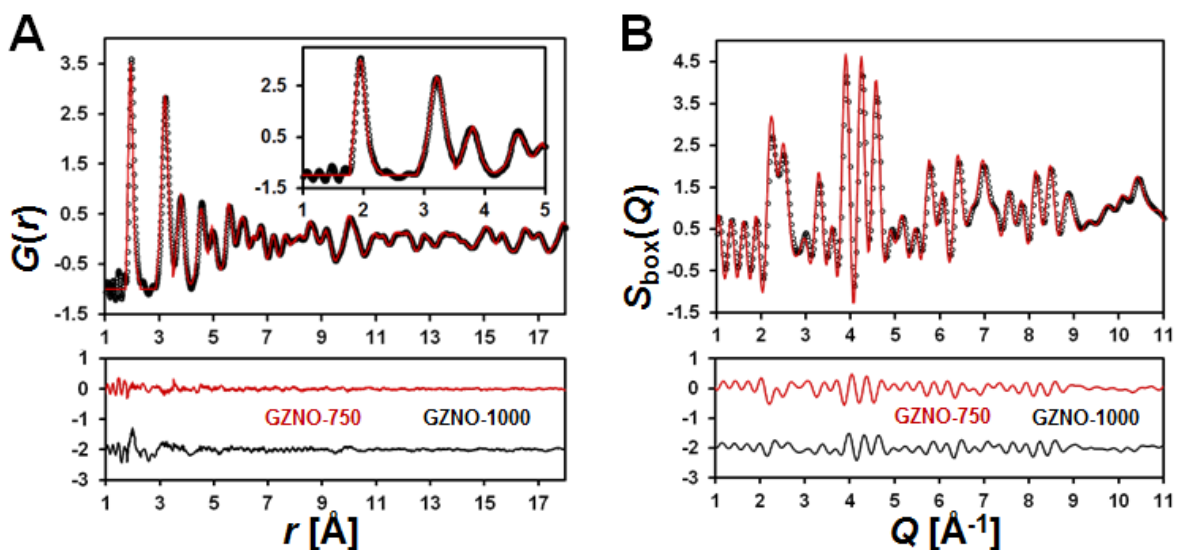
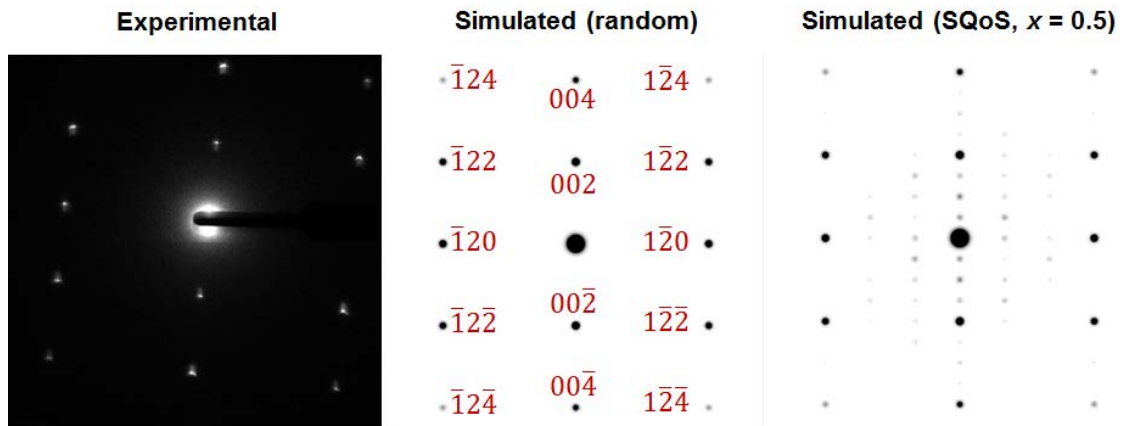


Figure S11. RMC refinement of the GZNO temperature series. (A) The experimental $G(r)$ of GZNO-750 (open circles) fitted to the calculated pattern derived from the RMC structure model (red trace). The difference plot between the experimental and calculated $G(r)$ for GZNO-750, and GZNO-1000 is shown below the $G(r)$ plot. (B) The box-convolution of the experimental $S(Q)$ of GZNO-buff (open circles) fitted to the calculated pattern derived from the RMC structure model (red trace). The difference plot between the experimental and calculated $S(Q)$ for GZNO-750 and GZNO-1000 is shown below the $S(Q)$ plot.

Table S4. Residual values from the RMC refinement of the GZNO temperature series. Chi values from RMC refinements where the atom swapping was allowed were compared with refinements that had a random atomic arrangement and only allowed to translate.

Refinement	overall χ^2	Bragg χ^2	$G(r)$ χ^2	$S(Q)$ χ^2	BVS χ^2
GZNO-750	238.2	39.91	15.69	1654	0.24928
GZNO-750 (random)	239	39.87	15.72	1660	0.26825
GZNO-1000	241	51.81	13.82	1645	0.22
GZNO-1000 (random)	242	53.11	13.91	1648	0.24891

(100)



(201)

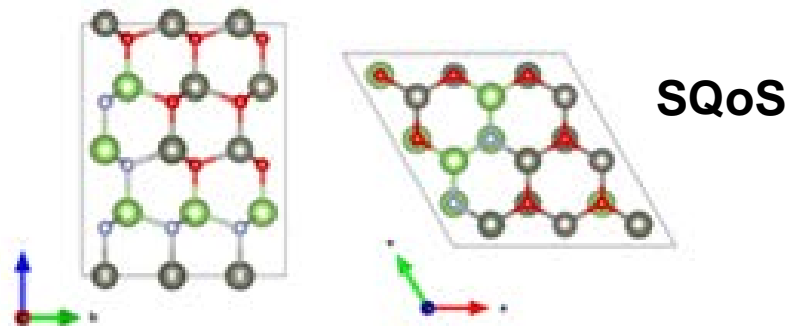
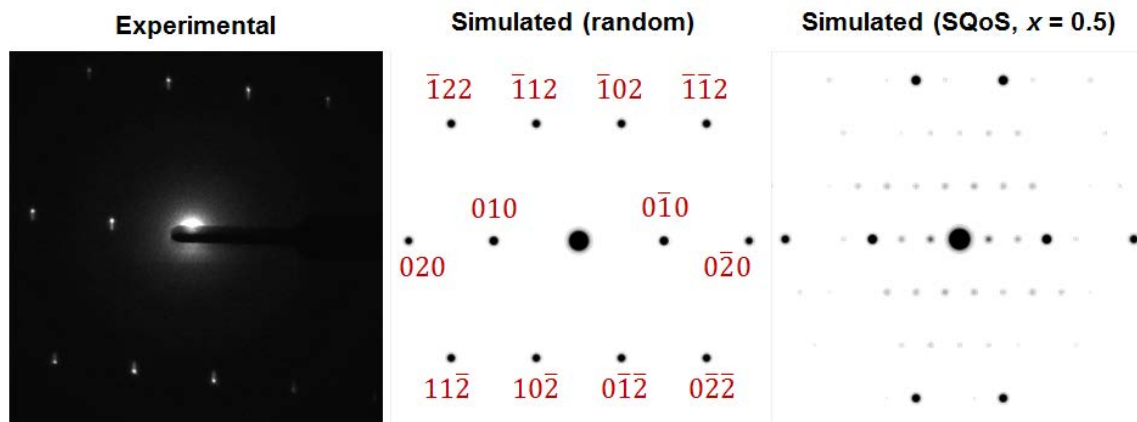


Figure S12. Representative SAED patterns of GZNO-buff obtained normal to the (100) and (201) plane are shown in the top left and bottom left panel, respectively. The corresponding electron diffraction patterns simulated from the wurtzite structure type (middle) and the Special Quasi-ordered Structure (SQoS) supercell (right) are also shown for comparison.²

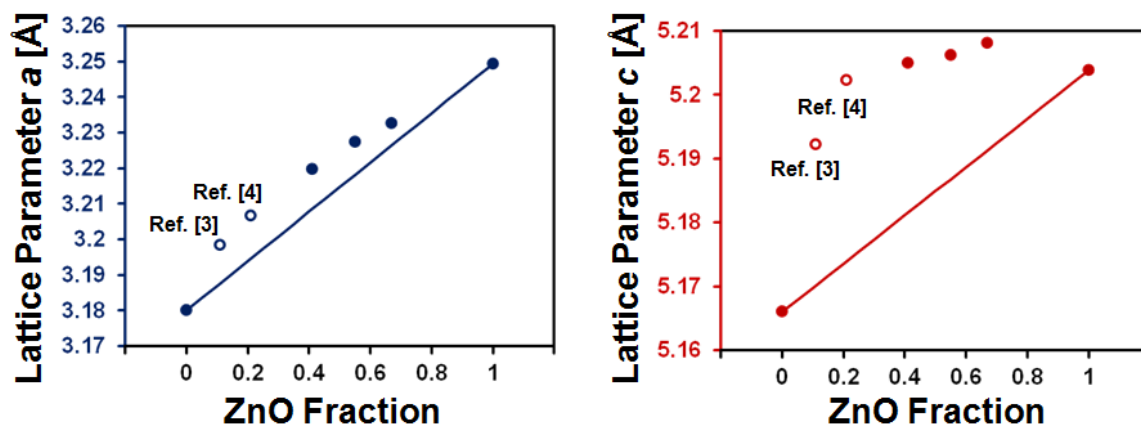


Figure S13. Filled circles represent GZNO unit-cell parameters obtained from Le Bail refinements using synchrotron diffraction data from 11-BM. Open circles refer to data obtained from ref. [3] and [4].

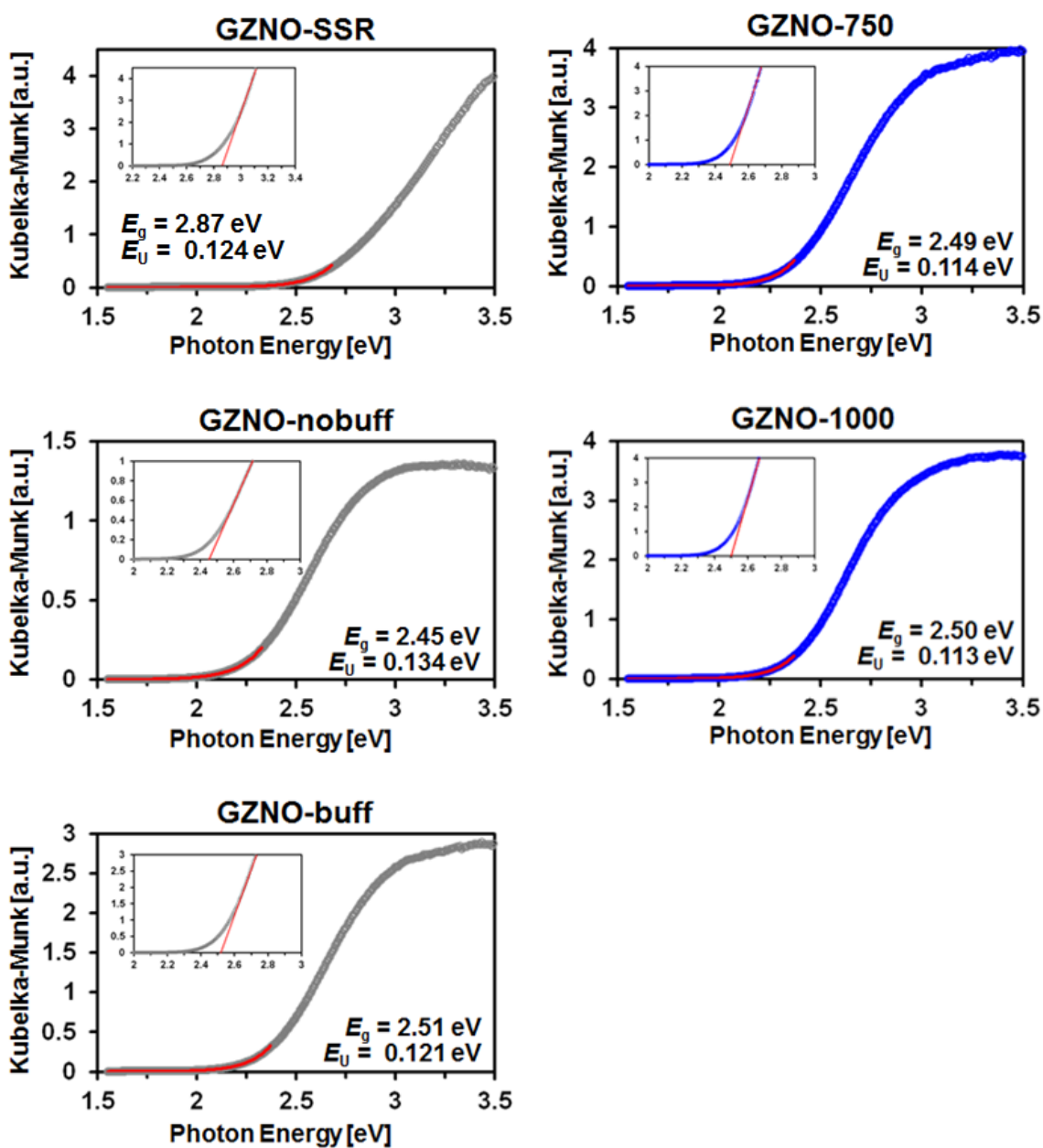


Figure S14. Kubelka-Munk transforms of the diffuse reflectance spectra of GZNO samples fitted to the Urbach equation for the derivation of the empirical E_U parameter tabulated in the main text. Shown in the inset are direct E_g Tauc plots where the linear region extrapolated to the abscissa to determine the bandgap energy.

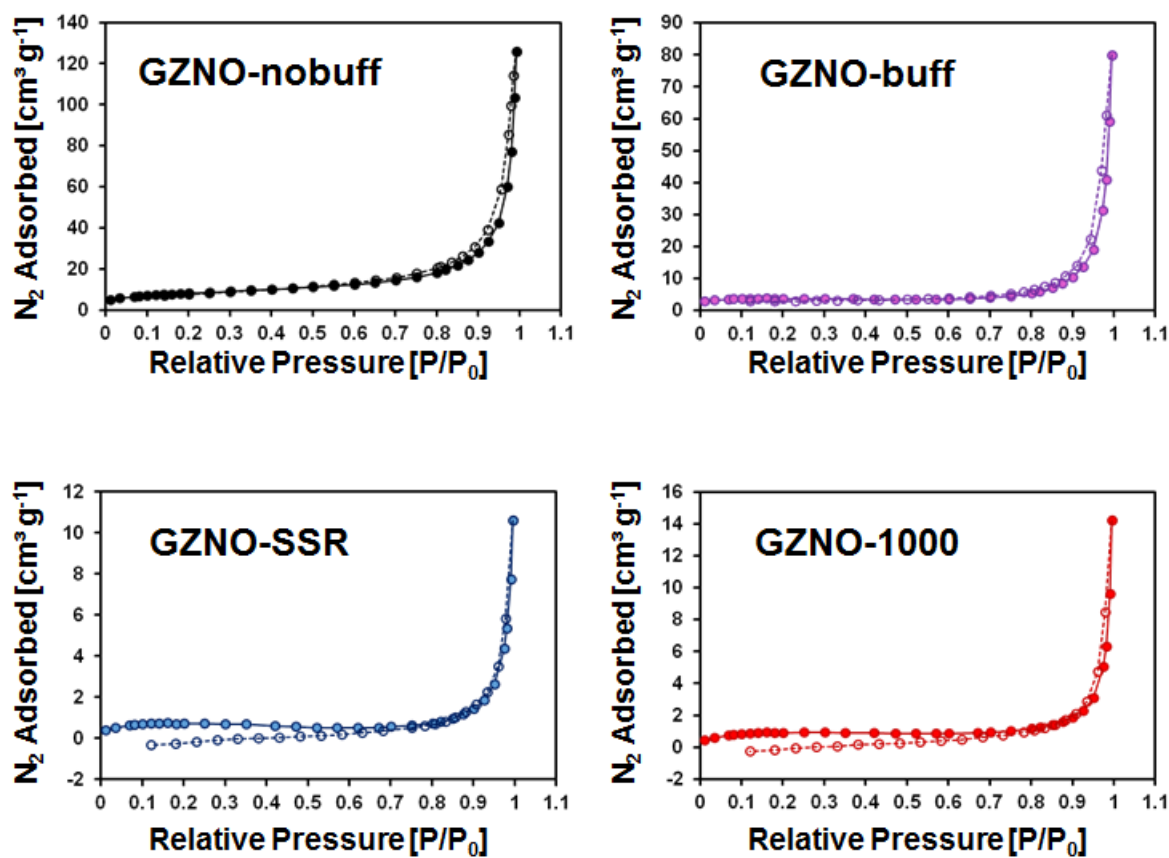


Figure S15. N₂ adsorption/desorption isotherms of the GZNO microcrystals used to obtain the Brunauer–Emmett–Teller (BET) surface areas. The surface-area specific activity in Figure 9 was obtained by normalization of the rate of oxygen evolution with the BET surface area. The filled and open markers correspond to the adsorption and desorption isotherm, respectively.

References

- (1) Balzar, D. Voigt-function model in diffraction line-broadening analysis. *Int. Union Crystallogr. Monogr. Crystallogr.* **1999**, *10*, 94–126.
- (2) Liu, J.; Fernández-Serra, M. V.; Allen, P. B. Special quasicrystalline structures: Role of short-range order in the semiconductor alloy (GaN)_{1-x}(ZnO)_x. *Phys. Rev. B* **2016**, *93*, 054207.
- (3) Yashima, M.; Yamada, H.; Maeda, K.; Domen, K. Experimental visualization of covalent bonds and structural disorder in a gallium zinc oxynitride photocatalyst (Ga_{1-x}Zn_x)(N_{1-x}O_x): origin of visible light absorption. *Chem. Commun.* **2010**, *46*, 2379–2381.
- (4) Chen, D. P.; Skrabalak, S. E. Synthesis of (Ga_{1-x}Zn_x)(N_{1-x}O_x) with Enhanced Visible-Light Absorption and Reduced Defects by Suppressing Zn Volatilization. *Inorg. Chem.* **2016**, *55*, 3822–3828.